Development mechanisms and regional characteristics of the Asian monsoon system

Ruth Geen[1], **F. Hugo Lambert**[1] **and Geoffrey K. Vallis**[1]

[1]College of Engineering, Mathematics and Physical Sciences, University of Exeter, North Park Road, Exeter, Devon EX4 4QF, United Kingdom.

Key Points:

- In idealized simulations with zonal land-sea contrast a Matsuno-Gill pattern forms and travels east via advective and evaporative feedbacks.
- The development and eastward expansion of this circulation generates a similar spatial pattern of monsoon onset to that seen across Asia.
- We suggest that elements of monsoon change and variability may be understood through how forcings modulate these feedbacks.

Corresponding author: Ruth Geen, r.geen@exeter.ac.uk

Abstract

Asian monsoon rainfall impacts one third of the global population and predicting its variability and future change is of clear importance. However, the dynamics of even the climatological monsoon are not fully understood. Three independent subsystems are traditionally considered: the East Asian, South Asian, and Western North Pacific monsoons. Here we use idealized model simulations with east-west thermal contrast to explore the complex observed onset behavior of these subsystems. Our results suggest that the summertime 'stationary wave' monsoon circulation is not simply a passive response to insolation, but instead expands northwestwards and then eastwards via advective and evaporative feedbacks. In particular, our simulations indicate that onset over the Western North Pacific results from eastward extension of the summertime continental low via atmospheric feedbacks. We propose that the regional monsoons' responses to forcings may be understood by considering how these feedbacks are influenced by the background state.

Plain Language Summary

Asian monsoon rainfall impacts one third of the global population and predicting its year-to-year variations and future change is of clear importance. A first step towards this goal is to understand the controls on the monsoon in the present climate. Each summer, as the Asian continent warms, the prevailing winds abruptly reverse direction from north-easterly to south-westerly, bringing warm, moist air over the land and causing the onset of the monsoon rains. However, rain does not arrive and end simultaneously across the continent. Instead, seemingly unconnected shifts in rainfall location occur in different regions through the year. Here, we use model simulations with simplified continents, alongside observations, to explore the processes responsible. We find that the basic elements of the observed behavior are captured simply by including east-west land-sea contrast, with further details reproduced when a simple Tibetan Plateau is added. Importantly, we find that the different monsoon onset timings across the continent and ocean arise from how the monsoon circulation actively transports warm, moist air, and not purely from warming of the land and ocean by the sun.

1 Introduction

The Asian monsoon rains arrive in multiple stages. Differences in behavior across the continent (e.g. Fig. 1a), alongside interest in regional impacts, have resulted in the separate study of three distinct components to the monsoon: the East Asian, South Asian and Western North Pacific monsoons (B. Wang & LinHo, 2002). Interannual variability and patterns of future change in these sub-monsoons are key foci of research, motivated by the impacts on global food supply (Gadgil & Gadgil, 2006; Naylor et al., 2007; Cui & Shoemaker, 2018). However, the climatological evolution of these systems is still not fully understood (Hsu et al., 2014; Parker et al., 2016; Geen et al., 2020). One important finding is that monsoon onset is not a passive, steady-state response to warming of a continent by summer insolation. For example, simulations by Bollasina and Ming (2013) demonstrated that land-atmosphere feedbacks allow Indian monsoon onset to progress even when insolation and SSTs are held at their May-mean values.

Observations and state-of-the-art simulations show how monsoons evolve, but the complexity of the system makes it hard to identify mechanisms. Idealized modeling complements the study of observations, allowing continents, orography and physical processes to be added incrementally. Two idealized modeling approaches have commonly been used to study the monsoons: aquaplanets (Earth-like planets with an entirely water-covered surface), to explore controls on zonal-mean tropical rainfall location (Privé & Plumb, 2007) and its seasonality (Bordoni & Schneider, 2008, 2010; Geen et al., 2018, 2019); and steady-state experiments with continents or localized forcing, to explore drivers of the seasonal-mean summertime stationary-wave pattern (Matsuno, 1966; Gill, 1980; Rod-

well & Hoskins, 2001; Shaw, 2014). Recent studies have begun to include idealized continents in aquaplanet simulations with seasonal cycles (Zhou & Xie, 2018; Voigt et al., 2016), but these do not separate the roles of zonal vs meridional asymmetry, leaving a gap in understanding between theories that emerge from highly abstracted aquaplanets and results based on observations and comprehensive models.

This study has two goals. First, to connect idealized work exploring the response to a zonally-localized, steady-state forcing with work exploring the zonally-symmetric, time-evolving response to insolation. Second, to identify the basic ingredients (e.g., land, orography) responsible for the disparate subseasonal behavior of the Asian monsoon subsystems. Section 2 describes the simulations and datasets used. In Section 3 we examine the development of the monsoon across the continent in the observations and simulations. In Section 4, we show evidence that the monsoon sub-system behaviors result from how the summertime stationary-wave pattern develops and expands via feedbacks with moist static energy and convection. Section 5 summarizes our conclusions.

2 Methods

2.1 Idealized model simulations

We use the Isca modeling framework (Vallis et al., 2018) with a configuration similar to that of the Model of an Idealized Moist Atmosphere (Jucker & Gerber, 2017). The model uses the GFDL spectral dynamical core, the RRTM radiation scheme (Mlawer et al., 1997; Clough et al., 2005) and simple parameterizations of moist physics and convection (Frierson et al., 2006, 2007; O'Gorman & Schneider, 2008). RRTM calculates radiative heating based on the local humidity and temperature every 1 hour of model time. As is common in idealized models, clouds are not included in the parametrisations of radiation or moist processes. The insolation includes a seasonal and diurnal cycle, with a solar constant of $1360\mathrm{Wm}^{-2}$, an Earth-like obliquity of 23.429° and a circular orbit. Simulations are run at T42 resolution, with 40 vertical uneven sigma levels and a 720s timestep. Data is interpolated onto a pressure grid at 50-hPa spacing during post-processing. A 360-day calendar is used, so that each model month is 30 days and a year comprises 72 pentads. The model is spun-up for 10 years and then run for a further 30 years. Data from this 30 year period are then used to produce a climatology.

Results from three simulations are presented. In the first, *half-land*, we isolate the role of zonal thermal contrast. The entire Eastern Hemisphere (0 to 180°E, -90 to 90°N) is prescribed as land and the Western Hemisphere (-180 to 0°E, -90 to 90°N) as ocean. Land is given a mixed layer depth of 2m and albedo of 0.325, while ocean has a mixed layer depth of 20m and albedo of 0.25. The high albedos compensate for the lack of clouds in the model. Hydrology is not explicitly accounted for in this highly idealized set-up. Instead, similar to the TRACMIP protocol (Voigt et al., 2016), an evaporative resistance, α is used to modify evaporation, E, as

$$E = \alpha \rho_a C |\mathbf{v}_a| (q_s - q_a) \tag{1}$$

where ρ_a, $|\mathbf{v}_a|$ and q_a are the density, horizontal wind speed, and specific humidity at the lowest model level respectively. C is the drag coefficient and q_s is the saturation specific humidity at the surface temperature. Over ocean, $\alpha = 1$ and there is no resistance to evaporation; over land $\alpha = 0.7$. In the second simulation, *simple-Asia*, land is further confined to the Northern Hemisphere, and an idealized Tibetan Plateau is introduced, with height, z, described by Saulière et al. (2012):

$$z = z_0 e^{-\delta_1^2} (1/\delta_2) e^{-0.5(\ln \delta_2)^2} \tag{2}$$

$$\delta_1 = [(x - x_0)\cos(\gamma_1) + (y - y_0)\sin(\gamma_1)]/L_1 \tag{3}$$

$$\delta_2 = [-(x - x_0)\sin(\gamma_2) + (y - y_0)\cos(\gamma_2)]/L_2 \tag{4}$$

where $z_0 = 5700$m, $(x_0, y_0) = (130., 28.)$, $\gamma_1 = -49.5°$, $\gamma_2 = -18°$, and $L_1 = L_2 = 12.5°$ (see contours in Fig. 1, central column and Fig. 3). Gibbs ripples are smoothed over land and ocean following Lindberg and Broccoli (1996). While this slightly reduces the elevation, the orography is sufficient to generate a similar impact on the circulation to that seen in reanalysis. The last simulation, *half-land-sn2*, is configured as *half-land*, but with the orbital period doubled, so that the seasonal cycle progresses at half the rate, and mixed layer depths doubled, so that the amplitude of the SST seasonality remains similar. This allows processes paced by dynamics to be distinguished from those paced by insolation.

Key elements lacking from our simulations are clouds and a description of land hydrology. In spite of this, the experiments mimic much of the behavior seen in observations and reanalysis (Fig. 1). Simulations with a bucket hydrology (Manabe, 1969) were performed for comparison (Fig S1; discussed in Section 5).

2.2 Reanalysis and observations

The Japanese 55-year Reanalysis (JRA-55; Kobayashi et al., 2015) is used for winds, specific humidity, temperature, geopotential height and heat fluxes, while the CPC Merged Analysis of Precipitation (CMAP; Xie & Arkin, 1997) dataset is used for precipitation. These were selected for their long records of daily data and the use of 4Dvar data assimilation in JRA-55. Climatologies are evaluated for 1979-2016. Results were also checked using the ERA-5 (Hersbach et al., 2020) and GPCP (Huffman et al., 2001) datasets for 1997-2020 (Fig. S1).

3 Seasonal Progression of Monsoon Rain

Fig. 1 shows monsoon onset timing for the observations (left), *simple-Asia* (centre) and *half-land* (right), defined as the pentad at which rainfall exceeds the January mean by at least 5mm/day (B. Wang & LinHo, 2002). To help in interpreting the onset patterns, the rows below show maps of climatological-mean precipitation, 850-hPa wind vectors and geopotential height anomalies relative to the zonal mean.

The observations show the well-documented features of Asian monsoon onset (B. Wang & LinHo, 2002). Land warms relative to ocean through Spring, lowering the geopotential over the continent and setting up a circulation with westerlies across the south of the Asian continent and southwesterly flow across the Indochina Peninsula and along the East Asian coast. Prior to Asian monsoon onset, South China experiences spring rain from mid-March to May (Linho et al., 2008, and bright yellow in Fig. 1a). Monsoon rain intensifies first over the Bay of Bengal in pentad 25 (1-5 May), then extends across the South China Sea by pentad 28 (16-20 May). A subtropical front develops that extends from the South China Sea to the ocean south of Japan, associated with a south-west to north-east oriented band of earlier rain (Fig. 1a&d). By pentad 34 (15-19 June), the Asian low and Western North Pacific subtropical high set up three bands of rain meeting in the South China Sea: the monsoon trough across the Arabian sea, India and the Bay of Bengal; the tropical convergence zone over the Western North Pacific; and a subtropical front across East Asia (Meiyu/Baiyu). Through pentads 34-40 (mid-June to mid-July), rain expands northwestward over India, while the monsoon westerlies over India and the Bay of Bengal strengthen further (Fig. 1g&j), and the subtropical front migrates north and weakens. Towards the end of the summer (pentad 46, 14-18 August), the monsoon westerlies extend eastward and Western North Pacific precipitation shifts farther north (Fig. 1a&m).

The onset behavior in the observations is complex, and might be assumed to be the product of the specific configuration of the Asian continent and ocean basins. However, the idealized simulations suggest much of the behavior arises purely from east-west

thermal contrast. The right-hand column of Fig. 1 shows results for *half-land*. A band of earlier onset extends south-west to north-east from the centre of the continent up to the eastern coastline. Precipitation expands first northwestward, and later eastward out over the ocean. The maps in the panels below show that the warming of land through spring sets up a continental low, and southwesterlies develop along the eastern coast at the interface with the oceanic high (Fig. 1f). By pentad 38, similar to pentad 34 in the observations, three rainfall regimes can be seen, the monsoon trough over land, the tropical convergence zone over ocean, and a subtropical front across the coast. Differences arise in pentad 44-56 of the simulation. The region of most intense convection travels eastward and the continental low follows, resembling an eastward-propagating Matsuno-Gill circulation (Gill, 1980, Fig. 3).

In *simple-Asia*, land is limited to the Northern Hemisphere and an idealized Tibetan Plateau is added. In this case the earliest arrival of precipitation is in the areas to the south and east of the plateau, mimicking the behavior observed over the Bay of Bengal and South China respectively (Fig. 1b). As in *half-land*, a continental low develops (now with a minimum anchored by the Tibetan Plateau) and generates 3 bands of rainfall, meeting over the south-east corner of the continent. In this simulation the low expands eastward in pentads 44 and 50, bringing rain over the subtropical ocean (cf. pentads 40 and 46 in the observations), but unlike *half-land* this does not detach from the continent.

4 Circulation-Moisture Feedbacks

Monsoon flows involve complex interactions of the tropical overturning circulations with moist processes and the land surface, so building a conceptual understanding of the processes and feedbacks responsible for the onset stages seen in Fig. 1 is challenging. Moist static energy (MSE), h, describes an air parcel's potential energy and moist enthalpy:

$$h \equiv c_p T + gz + L_v q_v. \tag{5}$$

Here, c_p is the specific heat of air at constant pressure; T is temperature; g the gravitational constant; z geopotential height; L_v is the latent heat of vaporization of water and q_v is specific humidity. Theory developed in aquaplanets indicates that in monsoon flows where transient eddies are suppressed (Schneider & Bordoni, 2008) and the atmosphere is near convective quasi-equilibrium (CQE; Betts, 1982; Emanuel, 1995), then the divide between the zonal mean Hadley cells is co-located with the tropical maximum in subcloud MSE (Privé & Plumb, 2007). When this maximum occurs away from the Equator, the strongest convergence and rainfall lie nearby on its equatorward side. If these ideas can be extended to Earth's local tropical overturning, then the MSE budget can be used not just to diagnose where convection might occur, but to interpret how feedbacks with the circulation influence the seasonal migration of the ITCZ and monsoon rain.

Although strictly it is the subcloud MSE that is connected to the distribution of precipitation in the tropics (Privé & Plumb, 2007), because the tropical atmosphere is close to CQE the column-integrated MSE strongly reflects the low-level distribution (not shown). The vertically-integrated MSE budget has the advantage of indicating how the column is fed MSE by surface heat fluxes:

$$\frac{\partial\{\overline{\mathcal{E}}\}}{\partial t} = \overline{F}_{net} - \left\{\overline{u}\frac{\partial\overline{h}}{\partial x}\right\} - \left\{\overline{v}\frac{\partial\overline{h}}{\partial y}\right\} - \left\{\overline{\omega}\frac{\partial\overline{h}}{\partial p}\right\} - \nabla\cdot\{\overline{h'\mathbf{v}'}\} \tag{6}$$

$$\mathcal{E} \equiv c_v T + gz + L_v q_v \tag{7}$$

$$F_{net} \equiv LH + SH + R_{toa} + R_{surf}. \tag{8}$$

Here, $\mathcal{E}$ is the sum of internal, latent and potential energy and c_v is the specific heat of air at constant volume. u, v, and ω are the zonal, meridional, and vertical wind speeds,

and $\mathbf{v}$ is the horizontal wind vector. F_{net} is the net flux of energy from latent, LH, and sensible, SH, heat fluxes, and radiative fluxes at the top of atmosphere, R_{toa}, and surface, R_{surf} (sign convention is that fluxes directed into the atmosphere are positive, cf. Hill et al., 2017). Overbars indicate the local climatological pentad mean, and primes deviations from this. Braces indicate column-mass integrals: $\{X\} \equiv \int_0^{p_s} X dp/g$, where p_s is surface pressure.

Eq. 6 describes how the internal plus potential energy of an air column is affected by the net diabatic heat fluxes into the column, advection of MSE by the climatological mean flow, and transient eddy fluxes of MSE. The latter term was found to be comparatively small in magnitude and is not presented here. Note that Eq. 6 is derived as an approximation to the energy budget of an air parcel, assuming kinetic energy terms are small (Neelin, 2007). MSE is only approximately conserved and is distinct from $\mathcal{E}$, which uses c_v in place of c_p, accounting for pressure variations following the air parcel. The lefthand columns of Figs. 2, 3 and 4 show column integrated MSE (shading) and precipitation (blue contours), confirming that the tropical precipitation tends to lie just equatorward of the peak in column-integrated MSE, even when zonal asymmetries are included.

We start by analyzing the MSE budget of the *half-land* simulation, as the simplest step building on previous results in aquaplanets (Bordoni & Schneider, 2008). In Fig. 2a (pentad 32) the meridional peak in MSE and the ITCZ are still near the Equator. The land has warmed in the Northern Hemisphere and a cross-equatorial circulation has begun to develop here, as indicated by the slight northward displacement of the ITCZ. Over land, the net energy fluxes into the column (F_{net}) act to increase the MSE of the column further (Fig. 2b), while near the Equator, the meridional circulation (Fig. 2d) advects cooler, drier air up the MSE gradient, resulting in a net cooling (Fig. 2e). The result is a northward advance of the MSE peak and ITCZ by pentad 38 (Fig. 2f). These meridional processes at work over land are similar to those that have been identified in aquaplanets (Bordoni & Schneider, 2008). In contrast with the aquaplanets, the cyclonic monsoon flow forced by the warm land generates southwesterlies over the coastline (black contour) at $\sim 20°$N (Figs. 1f&i). These advect MSE down-gradient, warming and moistening the air columns over the ocean at $\sim 30°$N, and extending the MSE maximum eastward (Fig. 2c,e&f). Accompanying this, the precipitation near the coastline migrates off the Equator and the continental low extends eastward (Fig. 1i&l). Once the monsoon westerlies extend over the ocean, the increased surface wind speeds enhance evaporation (gray contours, Fig. 2l). This feeds moisture into the column, increasing the interhemispheric MSE contrast over the ocean (180-200°E) (Fig. 2f&k). In accordance with Privé and Plumb (2007) deep convection in the ascending branch of the Hadley cell follows the MSE maximum off the Equator, bringing rain over the western ocean. By pentad 44, the westerlies are advecting lower MSE air up-gradient, resulting in cooling and drying over the coastline (Fig. 2m&r). This causes the unrealistic detachment of the MSE peak, monsoon low and precipitation away from the coastline seen in Fig. 1o&r.

Monsoon rain does not detach from the continent in observations, but the eastward movement of the continental low in *half-land* by advective and evaporative feedbacks may shed light on the retreat of WNP high and advance of Asian low (Fig. 1m), motivating us to explore the behavior here further. Fig. S2 compares the monsoon's eastward propagation rate over the ocean in *half-land* with the *half-land-sn2* simulation, in which the year length is doubled so the insolation evolves more slowly. We find that the mature monsoon gyre propagates eastward at a similar rate in both simulations, confirming that the eastward travel of the monsoon is paced by feedbacks with the circulation, rather than the solar forcing.

To connect this highly idealized simulation back to the observed monsoon, Figs. 3 and 4 show results for *simple-Asia* and JRA-55 respectively. The patterns seen in *simple-Asia* are closer to those observed, suggesting the simulation captures the key ingredi-

ents of the system and provides a mid-point between the *half-land* simulation and JRA-55 data. Some similar processes are seen to those identified in *half-land*: MSE increases over land (Figs. 3&4 a,f&k) and the MSE maximum then propagates eastward via down-gradient MSE advection (Figs. 3&4 k&m) and evaporation of moisture by the monsoon westerlies (Figs. 3&4 p&q).

Important differences to the *half-land* simulation are evident in Figs. 3 & 4. As noted above, in *simple-Asia*, while precipitation extends eastward over ocean later in the season, it no longer detaches from the continent. This appears to result from two factors. First, the mechanical diversion of the wind around the orography forces a fixed low pressure centre which anchors the monsoon circulation (Fig. 1). Second, the ocean to the south retains heat for longer than the Southern Hemisphere land in the *half-land* simulation, so the MSE gradient reversal and advective cooling by the zonal flow seen in Figs. 2m&r do not occur.

A second significant difference is that the northward advance of MSE and precipitation over land are less zonally uniform in *simple-Asia* than *half-land*. MSE increases first to the south of the orography and its westward spread is delayed (e.g. compare Figs. 2 & 3a). These effects appear to be predominantly generated by the interaction of the Tibetan Plateau with the subtropical jet. At the beginning of the season (e.g. pentads 32-38) the Plateau generates southward flow on its Western side (Fig. 1e & h). This southward flow results in adiabatic descent, as indicated by the positive contribution of the meridional advection terms over India (Fig. 4d). This suggests that the earlier onset over the Bay of Bengal compared with India is not simply determined by enhanced moisture availability over the warm sea surface, but more by the delay of monsoon onset to the west by this dry subtropical inflow (cf. Parker et al., 2016). The Plateau also advances the arrival of subtropical precipitation to its east. Simulations in which the height of the Tibetan Plateau is systematically altered have shown that interactions between orography and the subtropical jet are key in generating the phases of the subtropical East Asian monsoon (Molnar et al., 2010; Chiang et al., 2020).

Simple-Asia does not perfectly capture the observed behavior. For example, in the observations, easterlies associated with the Pacific subtropical high bring lower MSE air up-gradient (e.g. Figs. 4g&m) and enhance surface evaporation over the ocean between 15-30°N (gray contours on F_{net} panels). These two processes appear to balance one another to give only a weak energy tendency over ocean (Figs. 4j&o). In addition, the diabatic column energy input over land is greater in the simulation than reanalysis, likely due to absent processes such as clouds or hydrology, discussed further below.

Overall, the idealized simulations highlight that the spatial and temporal structure of monsoon onset is to zeroth order a consequence of the circulation and feedbacks that emerge when zonal land-sea contrast meets a seasonal cycle, with the Tibetan Plateau further defining local characteristics. In particular, the simulations suggest that the extension of monsoon rain over the Western North Pacific is not a passive response to warming of the ocean through summer, but arises from dynamically-driven eastward expansion of the convection and monsoon low.

5 Discussion

Studies using aquaplanet simulations have shown how meridional circulation/MSE feedbacks can cause rapid poleward jumps in the location of tropical rain, similar to those seen over monsoon onset in South Asia and the South China Sea. However, the Asian monsoon shows complex local onset and withdrawal characteristics across the continent, extending to the subtropics. State-of-the-art climate models reproduce these observed characteristics, but leave the processes underlying its seasonal evolution unclear. The idealized simulations presented here allow us to identify new feedbacks in the zonal di-

rection, connecting results from aquaplanets to the observed system and bringing the focus back onto land-sea contrast as an essential component of the large-scale Asian monsoon. We find:

1. The detailed regional behaviors and longitudinal steps in rainfall observed over Asia arise fundamentally from zonal land-sea contrast; regional onset and withdrawal timing can be interpreted in terms of how a Matsuno-Gill-like circulation develops through the season.
2. The summertime stationary wave pattern does not develop passively in response to insolation, but actively interacts with MSE. Focussing on monthly or seasonal means in analysis of variability and future projections may obscure the dynamical drivers of precipitation timing and intensity.
3. Previous studies have considered the eastward progression of the monsoon over the Western North Pacific later in the season in terms of changes in SST (Wu, 2002). Our simulations instead suggest the monsoon circulation expands eastward at a rate set by feedbacks from advection of MSE and wind-induced evaporation.

While the idealized simulations are helpful in breaking down complex observed behavior they neglect some processes. In particular, our simulations do not include land-atmosphere feedbacks, known to be important to the northwestward propagation of the monsoon across India (Bollasina & Ming, 2013). Simulations with a bucket hydrology (cf. Manabe, 1969) were performed to assess the importance of land-atmosphere feedbacks to our conclusions (Fig. S1). Precipitation is inhibited over land with this hydrology, particularly in *half-land* with no ocean to the south. However, the basic features of monsoon development are still present in the *simple-Asia* simulation, albeit with the reduced precipitation delaying the pentad in which the onset criteria is met. Cloud radiative effects have been shown to influence monsoon onset in aquaplanet simulations (Byrne & Zanna, 2020) and are themselves strongly modulated by the monsoon circulation (Li et al., 2019; Huang et al., 2020). Clouds are absent in our simulations, but would be an interesting avenue for future work. In spite of these limitations our simulations capture key features of the observed behavior and help in interpreting the feedbacks responsible.

The perspective of the Global Monsoon (Trenberth et al., 2000; B. Wang & Ding, 2008) has proved useful in interpreting the coherent behavior of the northern and southern hemisphere monsoons on millennial timescales (L. Wang & Chen, 2014; Schneider et al., 2014). We suggest that our unified, non-stationary Matsuno-Gill perspective of the Asian monsoons might similarly provide a framework for interpreting patterns of variability and change. By altering the prevailing wind and temperature patterns, modes such as ENSO, or forcings from CO_2 and aerosols, will alter how the continental low develops and expands throughout the season. In addition, our *half-land* simulation is not specific to Asia, and it is likely that similar circulation/moisture interactions are important in other monsoon systems, providing a fundamental picture of a 'generic monsoon'.

Acknowledgments

The work was supported by the UK-China Research and Innovation Partnership Fund, through the Met Office Climate Science for Service Partnership (CSSP) China, as part of the Newton Fund. GKV also acknowledges support from the Leverhulme Trust (RPG 2015-186) and NERC (NE/M006123). Datasets for this research are available in these in-text data citation references: Japan Meteorological Agency/Japan (2013); NOAA/OAR/ESRL (1995); Copernicus Climate Change Service (C3S) (2017); Mesoscale Atmospheric Processes Branch/Laboratory for Atmospheres/Earth Sciences Division/Science and Exploration Directorate/Goddard Space Flight Center/NASA, and Earth System Science Interdisciplinary Center/University of Maryland (2018). Upon article acceptance, ideal-

ized model simulation data described in the study will be made available via the Open Research Exeter repository. For review purposes data has been uploaded to:

https://figshare.com/s/35cb0429d27661a27f3e

References

Betts, A. K. (1982). Saturation point analysis of moist convective overturning. *Journal of the Atmospheric Sciences*, *39*(7), 1484-1505. doi: 10.1175/1520-0469(1982)039⟨1484:SPAOMC⟩2.0.CO;2

Bollasina, M. A., & Ming, Y. (2013, Nov 01). The role of land-surface processes in modulating the indian monsoon annual cycle. *Climate Dynamics*, *41*(9), 2497–2509. Retrieved from `https://doi.org/10.1007/s00382-012-1634-3` doi: 10.1007/s00382-012-1634-3

Bordoni, S., & Schneider, T. (2008). Monsoons as eddy-mediated regime transitions of the tropical overturning circulation. *Nature Geoscience*, *1*(8), 515–519. doi: 10.1038/ngeo248

Bordoni, S., & Schneider, T. (2010). Regime Transitions of Steady and Time-Dependent Hadley Circulations: Comparison of Axisymmetric and Eddy-Permitting Simulations. *Journal of the Atmospheric Sciences*, *67*(5), 1643–1654. doi: 10.1175/2009JAS3294.1

Byrne, M. P., & Zanna, L. (2020). Radiative effects of clouds and water vapor on an axisymmetric monsoon. *Journal of Climate*, *33*(20), 8789–8811.

Chiang, J. C. H., Kong, W., Wu, C. H., & Battisti, D. (2020). Origins of East Asian Summer Monsoon Seasonality. *Journal of Climate*. doi: 10.1175/JCLI-D-19-0888.1

Clough, S. A., Shephard, M. W., Mlawer, E. J., Delamere, J. S., Iacono, M. J., Cady-Pereira, K., ... Brown, P. D. (2005). Atmospheric radiative transfer modeling: A summary of the AER codes. *Journal of Quantitative Spectroscopy and Radiative Transfer*, *91*(2), 233–244. doi: 10.1016/j.jqsrt.2004.05.058

Copernicus Climate Change Service (C3S). (2017). *ERA5: Fifth generation of ECMWF atmospheric reanalyses of the global climate.* Copernicus Climate Change Service Climate Data Store (CDS). Accessed 07/29/2021. Retrieved from `https://cds.climate.copernicus.eu/cdsapp#!/home`

Cui, K., & Shoemaker, S. P. (2018). A look at food security in China. *npj Sci Food*, *2*, 4. doi: 10.1038/s41538-018-0012-x

Emanuel, K. A. (1995). On Thermally Direct Circulations in Moist Atmospheres. *Journal of the Atmospheric Sciences*, *52*(9), 1529–1534. doi: 10.1175/1520-0469(1995)052⟨1529:OTDCIM⟩2.0.CO;2

Frierson, D. M. W., Held, I. M., & Zurita-Gotor, P. (2006). A Gray-Radiation Aquaplanet Moist GCM. Part I: Static Stability and Eddy Scale. *Journal of the Atmospheric Sciences*, *63*(10), 2548–2566. doi: 10.1175/JAS3753.1

Frierson, D. M. W., Lu, J., & Chen, G. (2007). Width of the Hadley cell in simple and comprehensive general circulation models. *Geophysical Research Letters*, *34*(18), 1–5. doi: 10.1029/2007GL031115

Gadgil, S., & Gadgil, S. (2006). The Indian monsoon, GDP and agriculture. *Econ. Polit. Weekly*, *41*, 4887-4895.

Geen, R., Bordoni, S., Battisti, D. S., & Hui, K. (2020). Monsoons, ITCZs and the Concept of the Global Monsoon. *Reviews of Geophysics*, *58*(4), e2020RG000700. doi: 10.1029/2020RG000700

Geen, R., Lambert, F. H., & Vallis, G. K. (2018). Regime Change Behavior During Asian Monsoon Onset. *Journal of Climate*, *31*, 3327–3348. doi: 10.1175/JCLI-D-17-0118.1

Geen, R., Lambert, F. H., & Vallis, G. K. (2019). Processes and Timescales in Onset and Withdrawal of 'Aquaplanet Monsoons'. *J. Atmos. Sci.*, *76*, 2357–2373.

405 doi: 10.1175/JAS-D-18-0214.1
406 Gill, A. E. (1980). Some simple solutions for heat induced tropical circulation. *Quar-*
407 *terly Journal of the Royal Meteorological Society*, *106*(449), 447–462. doi: 10
408 .1002/qj.49710644905
409 Hersbach, H., Bell, B., Berrisford, P., Hirahara, S., Hornyi, A., Muoz-Sabater, J., ...
410 Thpaut, J.-N. (2020). The ERA5 global reanalysis. *Q.J.R. Meteorol. Soc.*,
411 *146*(730), 1999–2049. doi: 10.1002/qj.3803
412 Hill, S. A., Ming, Y., Held, I. M., & Zhao, M. (2017). A moist static energy budget-
413 based analysis of the Sahel rainfall response to uniform oceanic warming. *Jour-*
414 *nal of Climate*, *30*(15), 5637–5660. doi: 10.1175/JCLI-D-16-0785.1
415 Hsu, H.-H., Zhou, T., & Matsumoto, J. (2014). East Asian, Indochina and West-
416 ern North Pacific Summer Monsoon - An Update. *Asia-Pacific J. Atmos. Sci.*,
417 *50*(1), 45–68. doi: 10.1007/13143-014-0027-4
418 Huang, M., Li, J., Zeng, G., & Xie, Y. (2020). Regional characteristics of cloud
419 radiative effects before and after the South China Sea summer monsoon onset.
420 *Journal of Meteorological Research*, *34*(6), 1167–1182.
421 Huffman, G. J., Adler, R. F., Morrissey, M. M., Bolvin, D. T., Curtis, S., Joyce, R.,
422 ... Susskind, J. (2001). Global Precipitation at One-Degree Daily Resolution
423 from Multisatellite Observations. *Journal of Hydrometeorology*, *2*, 36–50.
424 Japan Meteorological Agency/Japan. (2013). *JRA-55: Japanese 55-year Reanaly-*
425 *sis, Daily, 3-Hourly and 6-Hourly Data.* Boulder CO: Research Data Archive
426 at the National Center for Atmospheric Research, Computational and Infor-
427 mation Systems Laboratory. Retrieved from `https://doi.org/10.5065/`
428 `D6HH6H41`
429 Jucker, M., & Gerber, E. P. (2017). Untangling the annual cycle of the tropical
430 tropopause layer with an idealized moist model. *Journal of Climate*, *30*(18),
431 7339-7358. doi: 10.1175/JCLI-D-17-0127.1
432 Kobayashi, S., Ota, Y., Harada, Y., Ebita, A., Moriya, M., Onoda, H., ... Taka-
433 hashi, K. (2015). The jra-55 reanalysis: General specifications and basic char-
434 acteristics. *J. Meteorol. Soc. Jpn.*, *93*(1), 5-48. doi: 10.2151/jmsj.2015-001
435 Li, J., Wang, W.-C., Mao, J., Wang, Z., Zeng, G., & Chen, G. (2019). Persistent
436 spring shortwave cloud radiative effect and the associated circulations over
437 southeastern China. *Journal of Climate*, *32*(11), 3069–3087.
438 Lindberg, C., & Broccoli, A. J. (1996). Representation of topography in spectral
439 climate models and its effect on simulated precipitation. *Journal of Climate*,
440 *9*(11), 2641–2659. doi: 10.1175/1520-0442(1996)009⟨2641:ROTISC⟩2.0.CO;2
441 Linho, L. H., Huang, X., & Lau, N. C. (2008). Winter-to-spring transition in east
442 Asia: A planetary-scale perspective of the south China spring rain onset. *Jour-*
443 *nal of Climate*, *21*(13), 3081–3096. doi: 10.1175/2007JCLI1611.1
444 Manabe, S. (1969). Climate and the Ocean Circulation 1. *Monthly Weather Review*,
445 *97*(11), 739–774. doi: 10.1175/1520-0493(1969)097⟨0739:CATOC⟩2.3.CO;2
446 Matsuno, T. (1966). Quasi-Geostrophic Motions in the Equatorial Area. *J. Meteor.*
447 *Soc. Japan*, *44*(1), 25–43. doi: 10.2151/jmsj1965.44.1_25
448 Mesoscale Atmospheric Processes Branch/Laboratory for Atmospheres/Earth Sci-
449 ences Division/Science and Exploration Directorate/Goddard Space Flight
450 Center/NASA, and Earth System Science Interdisciplinary Center/University
451 of Maryland. (2018). *GPCP Version 1.3 One-Degree Daily Precipita-*
452 *tion Data Set.* Research Data Archive at the National Center for Atmo-
453 spheric Research, Computational and Information Systems Laboratory,
454 Boulder, Colo. (Updated monthly.) Accessed 08/03/2021. Retrieved from
455 `https://doi.org/10.5065/PV8B-HV76`
456 Mlawer, E. J., Taubman, S. J., Brown, P. D., Iacono, M. J., & Clough, S. A.
457 (1997). Radiative transfer for inhomogeneous atmospheres: RRTM, a vali-
458 dated correlated-k model for the longwave. *Journal of Geophysical Research*,
459 *102*(D14), 16 663–16 682. doi: 10.1029/97JD00237

Molnar, P., Boos, W. R., & Battisti, D. S. (2010). Orographic controls on climate and paleoclimate of Asia: thermal and mechanical roles for the Tibetan Plateau. *Annual Review of Earth and Planetary Sciences*, *38*(1), 77–102. doi: 10.1146/annurev-earth-040809-152456

Naylor, R. L., Battisti, D. S., Vimont, D. J., Falcon, W. P., & Burke, M. B. (2007). Assessing risks of climate variability and climate change for Indonesian rice agriculture. *Proceedings of the National Academy of Sciences*, *104*(19), 7752–7757. doi: 10.1073/pnas.0701825104

Neelin, J. D. (2007). Moist dynamics of tropical convection zones in monsoons, teleconnections, and global warming. *The Global Circulation of the Atmosphere*, *267*, 301.

NOAA/OAR/ESRL. (1995). *CPC Merged Analysis of Precipitation (CMAP).* Boulder CO: Research Data Archive at the National Center for Atmospheric Research, Computational and Information Systems Laboratory. Retrieved from `https://doi.org/10.5065/4QKP-PF57`

O'Gorman, P. A., & Schneider, T. (2008). Energy of Midlatitude Transient Eddies in Idealized Simulations of Changed Climates. *Journal of Climate*, *21*(22), 5797–5806. doi: 10.1175/2008JCLI2099.1

Parker, D. J., Willetts, P., Birch, C., Turner, A. G., Marsham, J. H., Taylor, C. M., ... Martin, G. M. (2016). The interaction of moist convection and mid-level dry air in the advance of the onset of the Indian monsoon. *Quarterly Journal of the Royal Meteorological Society*, *142*(699), 2256-2272. Retrieved from `https://rmets.onlinelibrary.wiley.com/doi/abs/10.1002/qj.2815` doi: 10.1002/qj.2815

Privé, N. C., & Plumb, R. A. (2007). Monsoon Dynamics with Interactive Forcing. Part I: Axisymmetric Studies. *Journal of the Atmospheric Sciences*, *64*(5), 1417–1430. doi: 10.1175/JAS3916.1

Rodwell, M. J., & Hoskins, B. J. (2001). Subtropical Anticyclones and Summer Monsoons. *Journal of Climate*, *14*(15), 3192–3211. doi: 10.1175/1520-0442(2001)014⟨3192:SAASM⟩2.0.CO;2

Saulière, J., Brayshaw, D. J., Hoskins, B., & Blackburn, M. (2012). Further Investigation of the Impact of Idealized Continents and SST Distributions on the Northern Hemisphere Storm Tracks. *Journal of the Atmospheric Sciences*, *69*(3), 840–856. doi: 10.1175/JAS-D-11-0113.1

Schneider, T., Bischoff, T., & Haug, G. H. (2014). Migrations and Dynamics of the Intertropical Convergence Zone. *Nature*, *513*(7516), 45–53. doi: 10.1038/nature13636

Schneider, T., & Bordoni, S. (2008). Eddy-Mediated Regime Transitions in the Seasonal Cycle of a Hadley Circulation and Implications for Monsoon Dynamics. *Journal of the Atmospheric Sciences*, *65*(1), 915–934. doi: 10.1175/2007JAS2415.1

Shaw, T. A. (2014). On the Role of Planetary-Scale Waves in the Abrupt Seasonal Transition of the Northern Hemisphere General Circulation. *Journal of the Atmospheric Sciences*, *71*(5), 1724–1746. doi: 10.1175/JAS-D-13-0137.1

Trenberth, K. E., Stepaniak, D. P., & Caron, J. M. (2000). The global monsoon as seen through the divergent atmospheric circulation. *Journal of Climate*, *13*(22), 3969–3993. doi: 10.1175/1520-0442(2000)013⟨3969:TGMAST⟩2.0.CO;2

Vallis, G., Colyer, G., Geen, R., Gerber, E., Jucker, M., Maher, P., ... Thomson, S. (2018). Isca, v1.0: A framework for the global modelling of the atmospheres of Earth and other planets at varying levels of complexity. *Geoscientific Model Development*, *11*, 843–859. doi: 10.5194/gmd-11-843-2018

Voigt, A., Biasutti, M., Scheff, J., Bader, J., Bordoni, S., Codron, F., ... Zeppetello, L. R. V. (2016). The Tropical Rain belts with an Annual Cycle and Continent Model Intercomparison Project: TRACMIP. *JAMES*, 1–64.

Wang, B., & Ding, Q. (2008). Global monsoon: Dominant mode of annual variation in the tropics. *Dynamics of Atmospheres and Oceans*, *44*(3), 165 - 183. doi: https://doi.org/10.1016/j.dynatmoce.2007.05.002

Wang, B., & LinHo. (2002). Rainy Season of the Asian-Pacific Summer Monsoon. *Journal of Climate*, *15*, 386–398. doi: 10.1175/1520-0442(2002)015%3C0386:RSOTAP%3E2.0.CO;2

Wang, L., & Chen, W. (2014). An intensity index for the East Asian winter monsoon. *Journal of Climate*, *27*(6), 2361–2374. doi: 10.1175/JCLI-D-13-00086.1

Wu, R. (2002). Processes for the northeastward advance of the summer monsoon over the Western North Pacific. *Journal of the Meteorological Society of Japan*, *80*(1), 67–83. doi: 10.2151/jmsj.80.67

Xie, P., & Arkin, P. A. (1997). Global Precipitation: A 17-Year Monthly Analysis Based on Gauge Observations, Satellite Estimates, and Numerical Model Outputs. *Bulletin of the American Meteorological Society*, *78*(11), 2539-2558. doi: 10.1175/1520-0477(1997)078⟨2539:GPAYMA⟩2.0.CO;2

Zhou, W., & Xie, S.-P. (2018). A Hierarchy of Idealized Monsoons in an Intermediate GCM. *Journal of Climate*, *31*, 9021–9036. doi: 10.1175/JCLI-D-18-0084.1

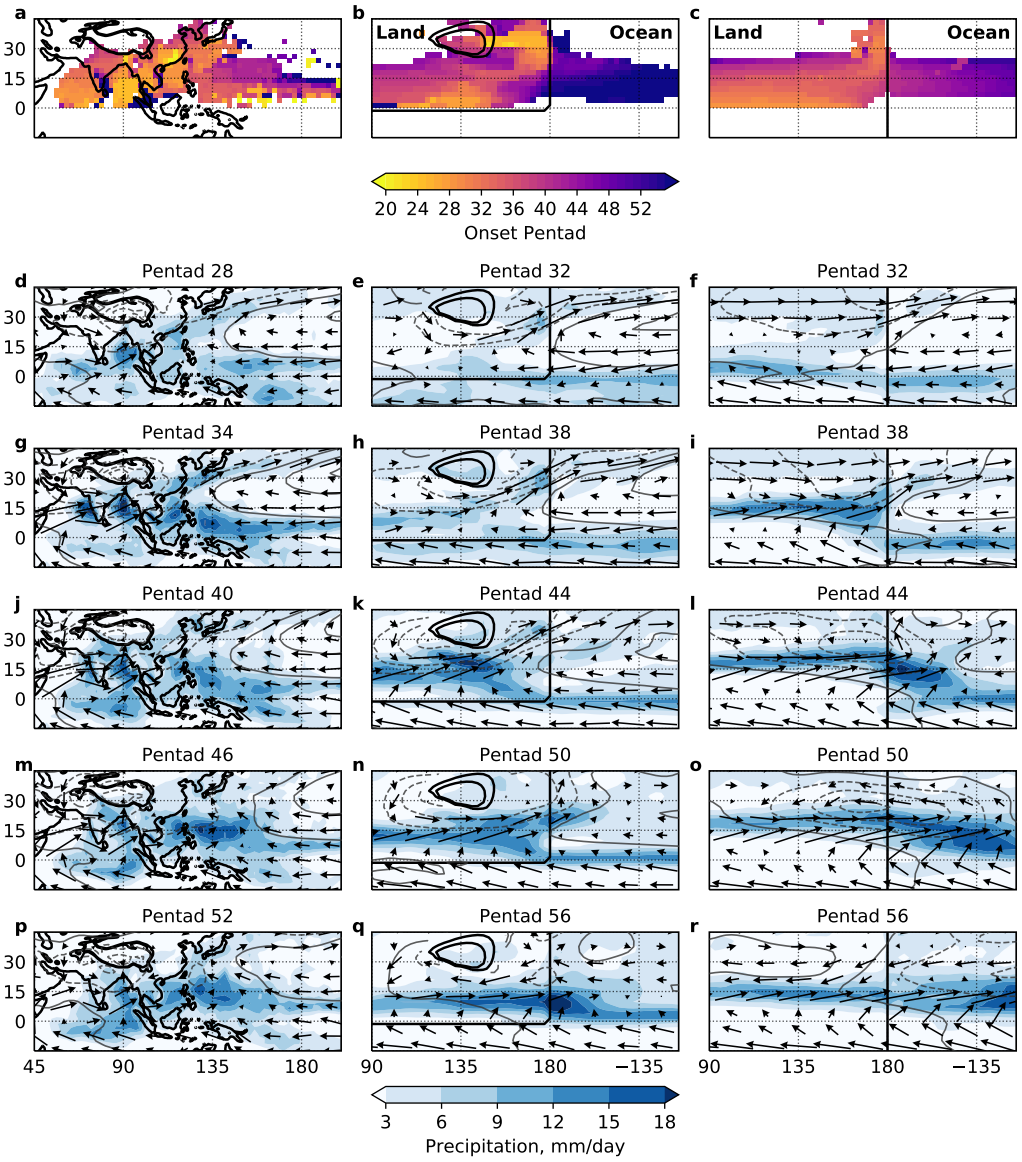

Figure 1. Top row shows Northern Hemisphere climatological monsoon onset pentad (B. Wang & LinHo, 2002). Lower rows show climatological mean precipitation (colors), 850-hPa wind (arrows) and 850-hPa geopotential height anomalies relative to the zonal mean (gray contours). The pentads used are indicated by the panel titles. Columns show results for (left) CMAP and JRA-55 data, (centre) *half-land*, (right) *simple-Asia*. Black contours show the coastlines and 2 and 3km orography contours.

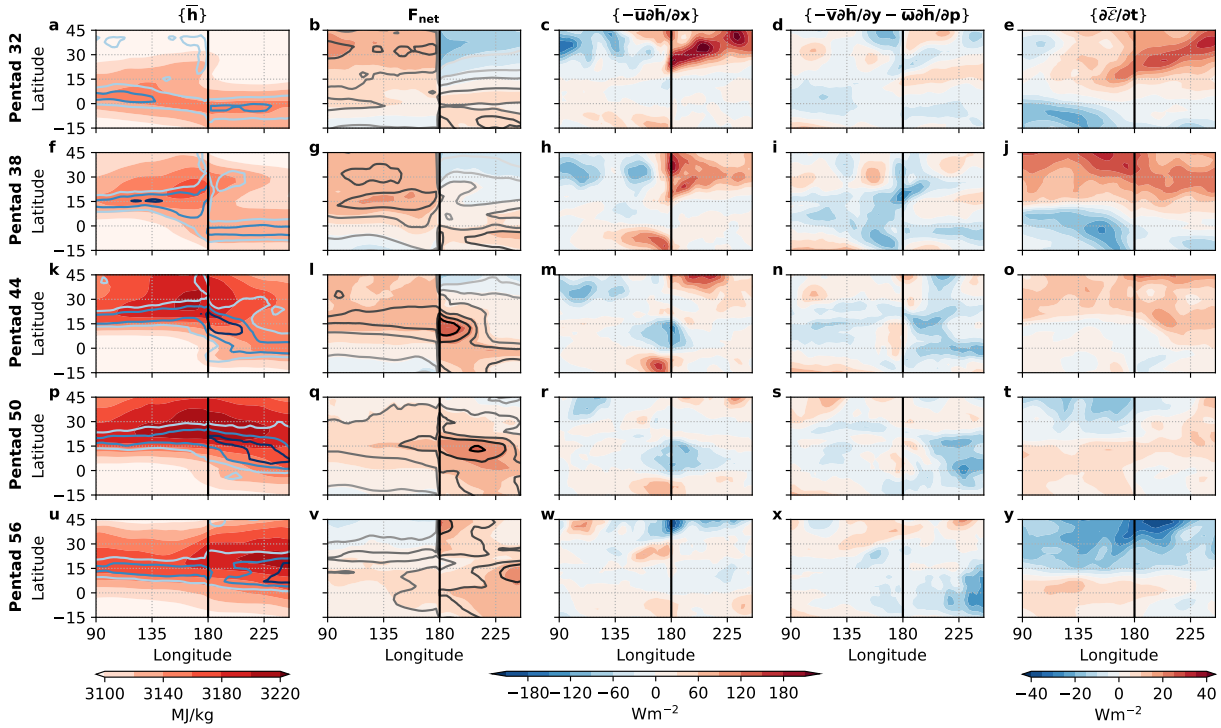

Figure 2. Maps of the column integrated MSE and the terms in the MSE budget (see Methods) for the *half-land* simulation. Black contours indicate the coastline. Blue contours in the lefthand column show precipitation, with interval 5 mm/day. Gray contours overlaid on $\overline{F}_{net}$ (second column) show the surface latent heat flux, with interval 30 Wm^{-2}. The terms and pentads shown are indicated by the column and row titles, respectively.

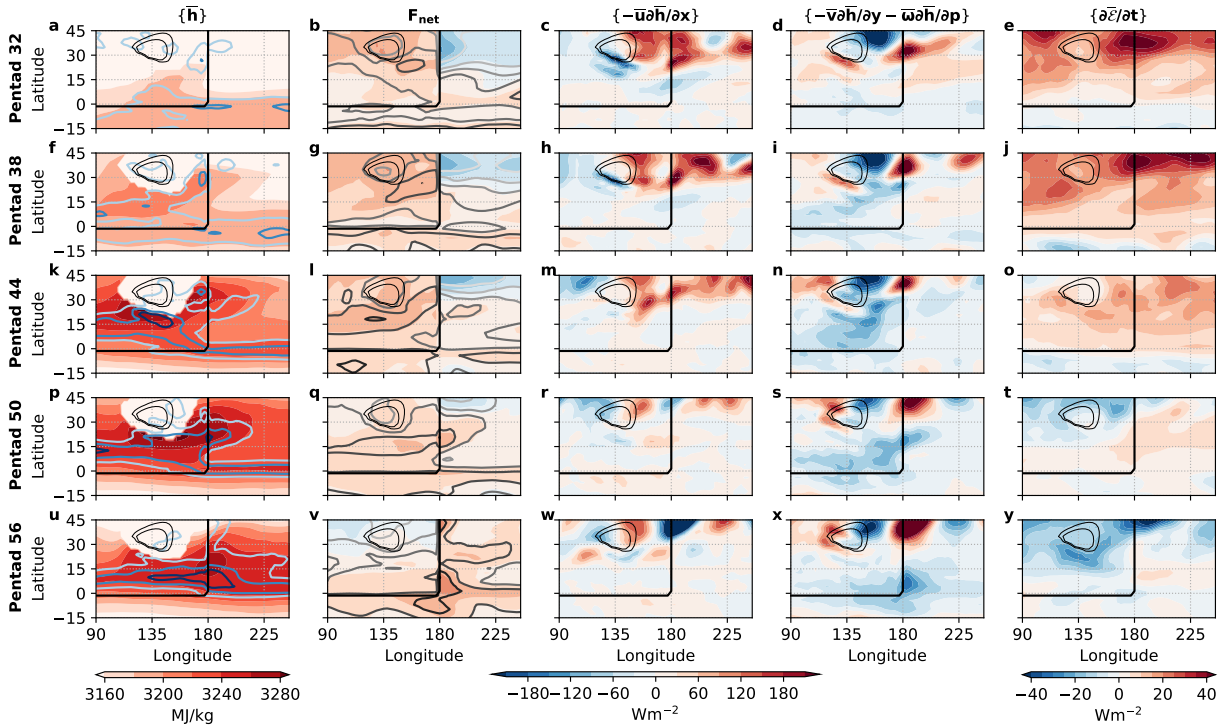

Figure 3. As Fig. 2, but for *simple-Asia*. Black contours show the coastline and 2 and 3km orography contours.

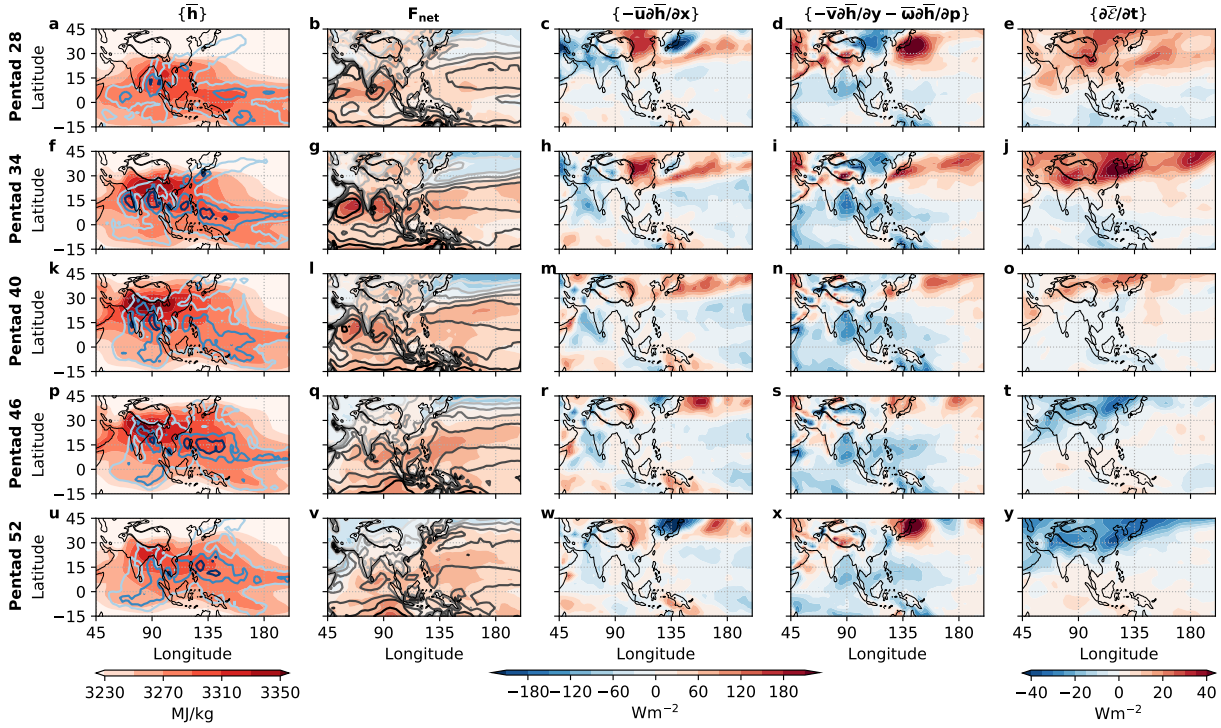

Figure 4. As Fig. 3, but for JRA-55 data, with CMAP precipitation contours in the lefthand column.